

NuSTAR observations of the ultraluminous X-ray source M33 X-8: a black hole in a very high state?

Roman Krivonos,^{1*} Sergey Sazonov,^{1,2*} Sergey S. Tsygankov,^{1,3*} and Juri Poutanen^{1,3,4*}

¹Space Research Institute of the Russian Academy of Sciences, Profsoyuznaya Str. 84/32, 117997 Moscow, Russia

²National Research University Higher School of Economics, Myasnitskaya ul. 20, 101000 Moscow, Russia

³Tuorla Observatory, Department of Physics and Astronomy, FI-20014 University of Turku, Finland

⁴Nordita, KTH Royal Institute of Technology and Stockholm University, Roslagstullsbacken 23, SE-10691 Stockholm, Sweden

4 June 2021

ABSTRACT

The closest known ultraluminous X-ray source (ULX), M33 X-8, has been recently observed with *NuSTAR* during its Extragalactic Legacy program, which includes a hard X-ray survey of the M33 galaxy. We present results of two long observations of M33 taken in 2017 March and July, with M33 X-8 in the field of view. The source demonstrates a nearly constant flux during the observations, and its 3–20 keV spectrum can be well described by two distinct components: a standard accretion disc with a temperature of ~ 1 keV at the inner radius and a power law with a photon index $\Gamma \approx 3$, which is significantly detected up to 20 keV. There is also an indication of a high-energy cutoff in the spectrum, corresponding to a temperature of the Comptonizing medium of $\gtrsim 10$ keV. The broad-band spectral properties of M33 X-8 resemble black hole X-ray binaries in their very high states, suggesting that M33 X-8 is a black hole accreting at a nearly Eddington rate, in contrast to super-Eddington accretion believed to take place in more luminous ULXs.

Key words: accretion, accretion discs – black hole physics – X-rays: binaries – X-rays: individual (M33 X-8)

1 INTRODUCTION

The first detailed X-ray studies of the individual source content of “normal” Local Group galaxies (distance $\lesssim 1$ Mpc) by the *Einstein* satellite have revealed a new class of intermediate luminosity ($L_X \gtrsim 10^{39}$ erg s⁻¹) X-ray sources (cf. Fabbiano 1989). Such objects, later found in larger numbers and at even higher ($\sim 10^{39}$ – 10^{41} erg s⁻¹) luminosities in more distant galaxies, are now widely referred to as ultraluminous X-ray sources (ULX, Makishima et al. 2000). Often, ULXs are defined as point-like off-nuclear sources whose apparent X-ray luminosity exceeds 10^{39} erg s⁻¹, which roughly corresponds to the Eddington limit for a “typical” stellar-mass ($\sim 10 M_\odot$) black hole (e.g., Long 1982; Fabbiano 1989; Marston et al. 1995; Colbert & Mushotzky 1999).

The nature of ULXs has been under debate for a long time. Extensive observations carried out in the standard 2–10 keV X-ray band have provided increasing evidence that most ULXs are stellar-mass black holes accreting in super-Eddington regime (see Feng & Soria 2011; Roberts et al. 2016, for reviews). In this case, the accretion disc is ex-

pected to be slim in its inner region, expelling some mass in a wind and collimating the radiation along the symmetry axis (Shakura & Sunyaev 1973; Lipunova 1999; Poutanen et al. 2007). At large viewing angles, the central source is hidden by the optically thick wind and its high luminosity may be revealed only through its impact on the surroundings, via photoionization or dynamical action of the outflowing material. Such a scenario is likely applicable to the microquasar SS 433 in our Galaxy (Fabrika 2004).

The discovery of periodic signals from a number of previously known ULXs (Bachetti et al. 2014; Fürst et al. 2016; Israel et al. 2017b,a) has provided strong evidence that a significant fraction of the ULX population may be powered by accretion onto a strongly magnetized neutron star. The disruption of the accretion disc by the stellar magnetic field at large radii can reduce the wind’s collimation efficiency because the disc then remains in sub-critical accretion regime (Lipunov 1982; Chashkina et al. 2017). The presence of pulsations also argues against strong collimation, because reprocessing in the wind would smear the signal. This implies that the dominant source of radiation is then not the accretion disc but accretion columns (Mushtukov et al. 2015, 2018) or an envelope around the neutron star (Mushtukov et al. 2017).

* E-mail: krivonos@iki.rssi.ru (RK); sazonov@iki.rssi.ru (SS); sergey.tsygankov@utu.fi (SST); juri.poutanen@utu.fi (JP)

There is growing evidence that the spectra of black-hole ULX and ULX-pulsars are different. Walton et al. (2018b) recently investigated the spectral signatures of the pulsed emission from three neutron-star ULXs, M82 X-2, NGC 7793 P13 and NGC 5907 ULX, finding that the accretion column (pulsed) emission in these sources dominates the total emission at high energies. Similar hard excesses are observed in a broader ULX sample with broadband coverage available to date, when the low-energy data are fitted with accretion disc models (e.g. Walton et al. 2013, 2014, 2015b). This suggests that a substantial fraction of the ULX population are neutron star accretors. We conclude that the broad-band spectroscopy becomes essential for understanding the nature of ULX central sources.

A salient ULX spectral feature, revealed by *XMM-Newton* observations, is a turnover of the X-ray spectrum above $\sim 5\text{--}10$ keV. This feature is not typical of normal (sub-Eddington) X-ray binaries (e.g. Zdziarski & Gierliński 2004; McClintock & Remillard 2006; Done et al. 2007) and strongly suggests that super-Eddington accretion takes place in ULXs. However, as *XMM-Newton* operates in the standard 2–10 keV X-ray band, observations of ULXs above 10 keV were highly anticipated to better constrain their spectra. The first attempt to perform imaging hard X-ray observations of ULXs, namely of M82 X-1 and Ho IX X-1, was undertaken by the *INTEGRAL* observatory (Winkler et al. 2003). These observations revealed a rollover above ~ 10 keV in the spectra of both sources (Sazonov et al. 2014). This fact was later confirmed by the *Nuclear Spectroscopic Telescope Array (NuSTAR)* (Brightman et al. 2016; Walton et al. 2014, 2017). *NuSTAR*, with its broad (3–79 keV) energy response, has opened a new era of hard X-ray observations of ULXs, providing a large set of broad-band ULX spectra (Walton et al. 2013, 2015a,b, 2018a; Mukherjee et al. 2015; Rana et al. 2015; Annuar et al. 2015; Krivonos & Sazonov 2016; Shidatsu et al. 2017).

M33 X-8 (Long et al. 1981; Trinchieri et al. 1988) is the closest known ULX. It has an X-ray luminosity of a few 10^{39} erg s^{-1} and is located in the nearby spiral galaxy M33 (=NGC 598) at a distance of ~ 817 kpc (e.g., Tüllmann et al. 2011). Although the position of the X-ray source is consistent with the center of M33 (Dubus & Rutledge 2002; Dubus et al. 2004), no activity in the nucleus of the galaxy has been revealed at other wavelengths. This testifies against an active galactic nucleus nature of M33 X-8. Furthermore, photometry and kinematics measurements of the nuclear region of M33 indicate that its central black hole, if any, has a mass less than $1500 M_{\odot}$ (Kormendy & McClure 1993; Merritt et al. 2001; Gebhardt et al. 2001). Finally, the discovery of the 106 days periodicity of M33 X-8 (Dubus et al. 1997) strongly contradicts the active galactic nucleus hypothesis and adds further evidence for an X-ray binary system, where modulations can be caused by precession of the accretion disc (e.g., Maloney et al. 1996). Note also that similar long-term periodicities have been recently detected in some ULX-pulsars (e.g. Walton et al. 2016).

M33 X-8 has been the subject of many studies (Gottwald et al. 1987; Trinchieri et al. 1988; Takano et al. 1994; Foschini et al. 2004; Weng et al. 2009; Middleton et al. 2011; Isobe et al. 2012; La Parola et al. 2015; Sutton et al. 2017). Most of the observations of the source were carried out at energies below 10 keV. The spectra measured in the

Table 1. List of *NuSTAR* observations of M33 X-8.

Date	ObsID	Exp. (ks)	Net count rate count s^{-1}	Total count
2017-03-06	50310002001	105.5	0.16	33800
2017-07-23	50310002003	101.8	0.14	28500

Note. The total number of counts is given as a sum of those detected by FPMA and FPMB.

2–10 keV band appear to be dominated by thermal emission from an optically thick, geometrically thin or slim accretion disc with a temperature of ~ 1 keV and allow for the presence of an additional power-law component with a photon index $\Gamma \approx 2$. The 2–10 keV spectrum of M33 X-8 thus resembles both the spectra of some other ULXs and those of Galactic black-hole binaries in their high and very high states. However, the narrowness of the energy band used for studying M33 X-8 so far allows for a lot of freedom in spectral modelling. It is thanks to the broad-band (3–79 keV) energy coverage of *NuSTAR* that we are able to reliably constrain the spectral components of M33 X-8 for the first time.

2 OBSERVATIONS AND DATA ANALYSIS

2.1 *NuSTAR*

The ULX M33 X-8 was observed with *NuSTAR* (Harrison et al. 2013) in 2017 during a hard X-ray survey of the nearby spiral galaxy M33 performed as part of the Extragalactic Legacy program.¹ *NuSTAR* carries two identical co-aligned X-ray telescopes with angular resolution of $18''$ (full width at half maximum, FWHM). The focal plane detector units of each telescope, referred to as focal plane modules A and B (FPMA and FPMB), cover a wide energy band 3–79 keV and provide spectral resolution of 400 eV (FWHM) at 10 keV.

The *NuSTAR* M33 survey consists of observations of the central region and the disc of the galaxy, carried out in two campaigns in 2017 March and July. We selected the central parts of the survey, listed in Table 1, where M33 X-8 was located within the *NuSTAR* FOV. The total exposure of the data set is 207 ks. Fig. 1 shows a mosaic sky map obtained by stacking the FPMA and FPMB images in the full 3–79 keV bandpass.

Because M33 X-8 produces a relatively high count rate of ~ 0.15 count s^{-1} on the *NuSTAR* detectors, we extracted the spectrum of the source from a large circular region with radius $R = 70''$, enclosing ~ 80 per cent of the point spread function (Madsen et al. 2015), centered at the position of M33 X-8 (RA=01:33:50.89, Dec=+30:39:37.2, J2000, Foschini et al. 2004). The *NuSTAR* spectrum was extracted using the NUPRODUCTS task of the *NuSTAR* Data Analysis Software (NUSTARDAS) v.1.8.0 and HEASOFT v6.22.1. The *NuSTAR* count rate within the $70''$ region is fully dominated by M33 X-8. Nevertheless, it can contain contributions from

¹ https://www.nustar.caltech.edu/page/legacy_surveys

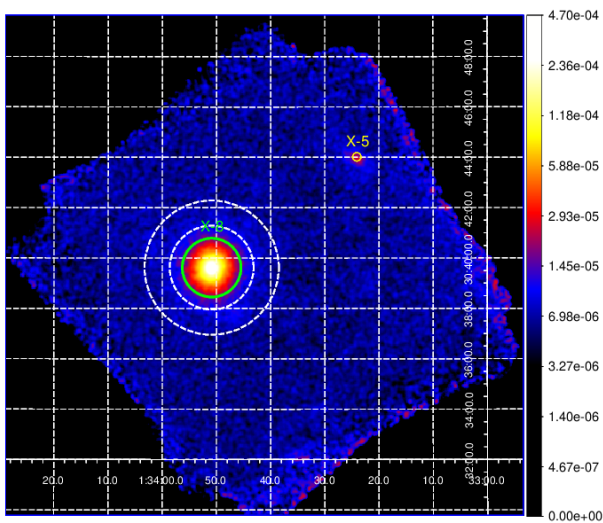


Figure 1. The *NuSTAR* count-rate image of the bulge of the M33 galaxy in the 3–79 keV energy band, with the total exposure of 207 ks. The solid green circle of radius $R = 70''$ denotes the region used for source spectrum extraction. The dashed annulus around it, limited by radii $R = 100'' - 160''$, shows the corresponding background region. The yellow region shows the position of the X-ray source M33 X-5 detected in the survey of M33 with *ROSAT* (Schulman & Bregman 1995).

other X-ray sources located within ~ 277 pc from M33 X-8 (projected distance corresponding to $70''$). The *Chandra* survey of M33 (Tüllmann et al. 2011) revealed three sources (SrcID. 321, 325 and 340) in the nuclear region within $70''$ from M33 X-8 (see Fig. 2). Their total flux in the 0.35–8.0 keV band (9.1×10^{-7} phot $s^{-1} \text{ cm}^{-2}$) is $\sim 2 \times 10^{-4}$ times that of M33 X-8 (4.3×10^{-3} phot $s^{-1} \text{ cm}^{-2}$, SrcID. 318). The background spectrum was extracted from the annulus region between $R = 100''$ and $R = 160''$ (Fig. 1). Within this region, there are 13 *Chandra* sources in the list of Tüllmann et al. (2011), with the total flux of 4.1×10^{-5} phot $s^{-1} \text{ cm}^{-2}$ in the 0.35–8.0 keV band, which corresponds to $\sim 3 \times 10^{-3}$ of the M33 X-8 flux (properly scaled to the area of the source region). We conclude that weak sources both within the *NuSTAR* source and background extraction regions do not significantly contaminate the measured flux of M33 X-8 in the 0.35–8.0 keV band and assume the same to be the case at higher energies.

2.2 *Swift*/XRT

The *Neil Gehrels Swift Observatory* (*Swift*) (Gehrels et al. 2004) has explored the central part of the M33 galaxy many times, targeting M33 X-8 (La Parola et al. 2015). We utilized data from the XRT telescope (Burrows et al. 2005) obtained during the long (~ 20 ks) on-axis observation of M33 X-8 in Photon Counting (PC) mode on 2012 November 5 (ObsID. 00031042002). It is the closest in time to the *NuSTAR* observations and of the best quality in terms of off-axis distance and exposure. The spectrum extraction was done using the online tools provided by the UK *Swift* Science Data Cen-

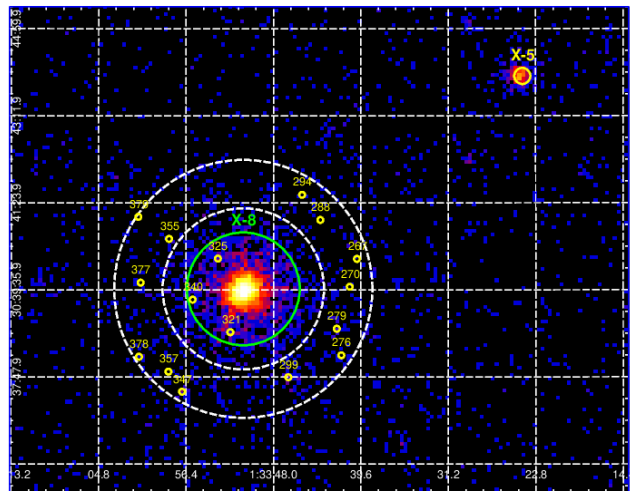


Figure 2. Same as Fig. 1, but for the *Swift*-XRT full-band (0.2–10 keV) photon counting image of M33 X-8. Yellow labels show the positions of X-ray sources detected in the *Chandra* survey of M33 (Tüllmann et al. 2011) within the *NuSTAR* source and background spectral extraction regions.

tre². The pile-up issues of M33 X-8 noticed by La Parola et al. (2015) have been resolved by the online spectrum extraction software (Evans et al. 2009). In particular, the code identifies those time intervals when the count rate is above 0.6 count s^{-1} within a 30 pixel radius around the source, builds the PSF profile of the source and compares it with the calibrated, non-piled-up PSF (Moretti et al. 2005). If the source is piled up, the algorithm excludes the inner PSF region affected by pile-up from the spectral extraction.

3 SPECTRAL ANALYSIS

3.1 General procedure

The spectral analysis was done using the X-ray Spectral Fitting Package (*XSPEC ARNAUD* 1996), version 12.9.1, part of the *HEASOFT* software package (version 6.22.1). The fitting procedures were conducted with spectra grouped to a minimum of 30 counts per bin to allow the use of χ^2 statistics. We quote errors at 90 per cent confidence intervals unless stated otherwise.

Each spectral model discussed below has an absorption component (PHABS), with the abundances adopted from Anders & Grevesse 1989) and the absorbing line-of-sight column density fixed at the Galactic value $N_{\text{H}} = 1.1 \times 10^{21} \text{ cm}^{-2}$ (Kalberla et al. 2005). An intrinsic absorption, if required by the fitting procedure, is included as a second PHABS component with a free column density parameter.

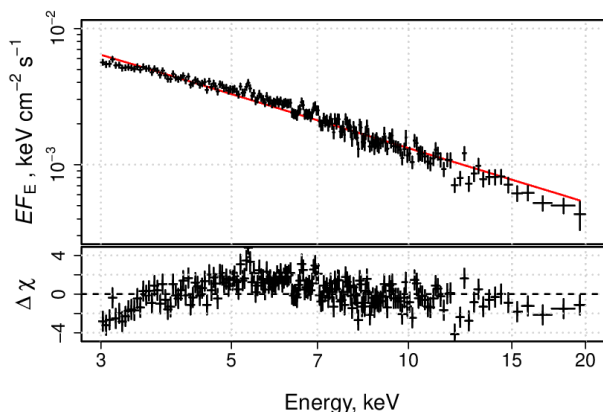
To estimate possible variability of M33 X-8 between the two epochs of *NuSTAR* observations (see Table 1), we fitted the 3–20 keV spectra by a simple power-law model without any intrinsic absorption, as summarized in Table 2. A cross-calibration coefficient between the FPMA and FPMB detectors was included in the fit and indicated that the FPMB

² <http://www.swift.ac.uk>

Table 2. Best-fit parameters for a power-law model obtained for both epochs of the *NuSTAR* observations in the 3–20 keV energy band.

Parameter	Units	Epoch 1	Epoch 2
CONSTXPOWERLAW			
Constant ^a		1.08 ± 0.02	1.01 ± 0.02
Γ		3.29 ± 0.03	3.36 ± 0.03
N_{pow}	10 ⁻² @1 keV	2.69 ± 0.12	2.92 ± 0.14
$F_{3-20 \text{ keV}}^{\text{pow}}$	10 ⁻¹² erg s ⁻¹ cm ⁻²	7.36 ± 0.11	7.11 ± 0.12
χ^2/dof		483/386	453/352

^aThe cross-calibration constant term is fixed at unity for FPMA and fitted for FPMB.

**Figure 3.** Average *NuSTAR* X-ray spectrum of M33 X-8 obtained during the observations in 2017 (black crosses) and approximated by a power law (red line) with a photon index $\Gamma = 3.32 \pm 0.02$ and normalization $N_{\text{pow}} = (2.8 \pm 0.1) \times 10^{-2}$, giving $\chi^2/\text{dof} = 924/739$.

spectrum had an 8 per cent higher normalization than the FPMA one in Epoch 1. This difference is somewhat larger than expected (0–5 per cent, Madsen et al. 2015). The epoch 2 FPMA/FPMB spectra have almost identical normalizations (with a difference of ~ 1 per cent). We fixed the relative normalization between the *NuSTAR* modules at these values for the following analysis. We also truncated the *NuSTAR* spectra above 20 keV, where the source spectrum is dominated by the background. As seen from Table 2, the best fitting parameters of the power-law model indicate low variability between the two epochs. The slope of the epoch 2 spectrum is marginally steeper, and there is a slight decrease in the 3–20 keV flux. We then combined both epochs into one data set to improve the statistics and to obtain a time-averaged broad-band spectrum of M33 X-8. Note that we did not co-add spectra and response files according to the *NuSTAR* Help Desk recommendations³, but rather fitted the individual spectra simultaneously. We stack *NuSTAR* spectra to one group for plotting purposes only.

³ https://heasarc.gsfc.nasa.gov/docs/nustar/nustar_faq.html

The *Swift*/XRT long observation of M33 X-8 is used to extend the broad-band spectrum to energies below 5 keV, where the effective area of *NuSTAR* drops rapidly (Madsen et al. 2015). In order to take into account possible source flux variations, we introduced a cross-normalization constant between the *Swift*/XRT and *NuSTAR* data.

3.2 Simple models

We first fitted the *NuSTAR* spectrum alone using a simple power-law model, as shown in Fig. 3. The fit is poor with $\chi^2 = 924$ for 739 degrees of freedom (dof). The best fitting spectral index $\Gamma = 3.32 \pm 0.02$ is consistent with that reported in Table 2 for both epochs of the *NuSTAR* observations. A significant curvature is evident over the 3–20 keV band, as shown in the lower panel of Fig. 3.

We next fitted the broad-band 0.3–20 keV *Swift*/XRT and *NuSTAR* data using a number of phenomenological models. We start with simple continuum models modified by additional intrinsic absorption if required by the fit. The list of the models contains: (1) a power-law model; (2) a power law with an exponential cutoff (CUTOFFPL); (3) a multi-colour disc model with the radial temperature dependence r^{-p} , with p being a free parameter (DISKPB, Mineshige et al. 1994); (4) a power law combined with a standard multi-colour disc model (DISKBB, Shakura & Sunyaev 1973); (5) a power law with an exponential cutoff (CUTOFFPL) combined with DISKBB. Table 3 lists the best fitting parameters and Fig. 4 shows the statistical residuals for each model.

The power-law fit for the broad-band spectrum demonstrates strong curvature variations over the 0.3–20 keV energy band, as shown in the upper panel of Fig. 4. The quality of the fit is poor ($\chi^2/\text{dof} = 1690/903$), although the power-law parameters are generally consistent with those derived for the *NuSTAR* data set alone (Fig. 3). The second model, with a power law modified by a high-energy exponential cutoff substantially improves the fit to $\chi^2/\text{dof} = 1207/902$, revealing an energy rollover at ~ 5 keV. This model, however, still has significant deviations from the data over the considered energy band.

The third model, a modified version of the multi-colour disc model, is often used in the literature to describe ULX spectra, including M33 X-8 (e.g. Isobe et al. 2012). This single-component model does not fit the broad-band data ($\chi^2/\text{dof} = 1584/902$), leaving a strong excess at energies above 10 keV, as shown in the middle panel of Fig. 4. Similar high-energy tails seen in *NuSTAR* observations of other ULXs (Walton et al. 2013, 2014, 2015b; Mukherjee et al. 2015) are usually attributed to Comptonization of accretion disc photons by a hot corona.

The fourth model, a combination of a power law and an accretion disc component DISKBB significantly improves the fit ($\chi^2/\text{dof} = 951/901$) revealing a power-law-like excess with $\Gamma = 2.54 \pm 0.08$ above 10 keV. However, the fitting residuals still demonstrate substantial variations, as evident in Fig. 4. The power-law photon index Γ and the inner disc temperature are consistent with the results of previous studies of M33 X-8, where a similar spectral model and data from *Swift*/XRT (La Parola et al. 2015), *XMM-Newton* (Foschini et al. 2004), or *Suzaku* (Isobe et al. 2012) were used. The innermost disc radius, R_{in} , can be directly estimated from the normalization of the DISKBB component: $N_{\text{disc}} = R_{\text{in}}^2 \cos i / D^2$,

Table 3. Best fitting parameters for a number of phenomenological models of the broad-band 0.3–20 keV *Swift*/XRT and *NuSTAR* spectrum.

Parameter	Units	Value
Model 1: PHABS×CONST×POWER-LAW		
N_{H}	10^{22} cm^{-2}	0.59 ± 0.04
Constant ^a		0.52 ± 0.03
Γ		3.32 ± 0.02
N_{pow}	10^{-2} @1 keV	2.9 ± 0.1
χ^2/dof		1690/903
Model 2: PHABS×CONST×CUTOFFPL		
N_{H}	10^{22} cm^{-2}	0.25 ± 0.03
Constant		0.80 ± 0.04
Γ		2.0 ± 0.1
E_{fold}	keV	4.7 ± 0.4
N_{cut}	10^{-2} @1 keV	1.0 ± 0.1
χ^2/dof		1207/902
Model 3: PHABS×CONST×DISKPB		
N_{H}	10^{22} cm^{-2}	0.18 ± 0.01
Constant		0.99 ± 0.04
kT	keV	1.88 ± 0.02
p		0.5 (hard limit)
N_{disk}	10^{-2}	2.0 ± 0.1
$R \cos^{1/2} i$	km	11 ± 1
χ^2/dof		1584/902
Model 4: PHABS×CONST×(DISKBB+POWERLAW)		
N_{H}	10^{22} cm^{-2}	0.17 ± 0.03
Constant		1.00 ± 0.04
kT	keV	1.21 ± 0.02
N_{disk}		0.21 ± 0.02
$R \cos^{1/2} i$	km	37 ± 2
Γ		2.54 ± 0.08
N_{pow}	10^{-3} @1 keV	3.1 ± 0.6
χ^2/dof		951/901
Model 5: PHABS×CONST×(DISKBB+CUTOFFPL)		
N_{H}	10^{22} cm^{-2}	$< 5^a$
Constant		1.03 ± 0.04
kT	keV	1.05 ± 0.03
N_{disk}		0.50 ± 0.08
$R \cos^{1/2} i$	km	58 ± 5
Γ		1.0 ± 0.3
E_{fold}	keV	5.3 ± 0.4
N_{cut}	10^{-4} @1 keV	7 ± 3
χ^2/dof		891/900

^a The 2σ upper limit.

where D is the distance to the source in units of 10 kpc and i is the inclination of the disc. The estimated inner disc radius, $R_{\text{in}} = (37 \pm 2) \cos^{-1/2} i$ km, is in good agreement with the results of previous studies (e.g., Middleton et al. 2011). Associating this size with the radius of the innermost stable orbit of a standard accretion disc suggests that the relativistic compact object has a mass of at least $\sim 4 M_{\odot}$, with the exact value depending on the (unknown) inclination of the disc. More accurate estimation should take into account the inner boundary condition, the spectral hardening and

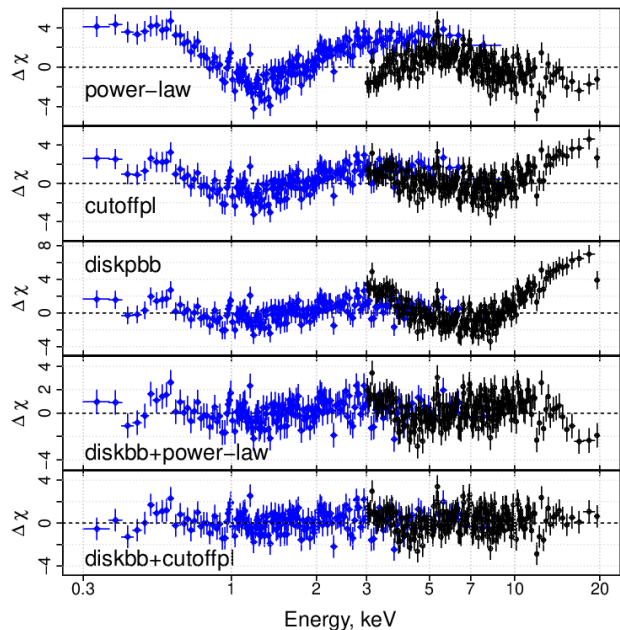


Figure 4. Residuals for the phenomenological spectral models considered in this study (from top to bottom): a power law, a power law with an exponential high-energy cut-off, multi-colour disc with the r^{-p} temperature profile, a combination of a standard accretion disc and a power law, and a combination of a standard accretion disc and a power law with an exponential high-energy cutoff. Blue diamonds and black circles show the *Swift*/XRT and *NuSTAR* data points, respectively.

relativistic corrections, which in turn would depend on the structure of the accretion disc (whether it is thin or slim). Nevertheless, the above crude estimate is consistent with the compact object being a stellar-mass black hole.

Replacing the power-law component by its modification with an exponential cutoff (Model 5) further improves the fit statistics to $\chi^2/\text{dof} = 891/900$, indicating the presence of a high-energy cutoff in the spectrum (the F-test probability is 10^{-14} for the null-hypothesis Model 4).

We conclude that the broad-band 0.3–20 keV spectrum of M33 X-8 cannot be described by a single accretion disc model DISKPB, which was previously used to successfully fit some narrow-band spectra of this source (e.g. La Parola et al. 2015). The broad-band spectrum strongly requires an additional power-law component with a possible high-energy cutoff.

3.3 Physically motivated models

We have demonstrated that the broad-band spectrum of M33 X-8 certainly contains two components: the first one is well approximated by a multi-colour disc with the inner temperature of $kT \sim 1$ keV, and the second one is a power-law-like high energy tail detected up to 20 keV. As often discussed in the literature (e.g. Gierliński et al. 1999; Steiner et al. 2009), the combination of a low-energy blackbody-like component with a high-energy power law does not allow one to properly model the spectrum at low energies, because a steep power law extending to the soft part of the spectrum

Table 4. Same as Table 3, but for Models 3a and 3b.

Parameter	Units	Value
Model 3a: CONST×SIMPL⊗DISKPBB		
Constant		0.87 ± 0.04
kT	keV	0.9 ± 0.1
p		0.77 ± 0.03
N_{diskpbb}		1.4 ± 0.4
$R \cos^{1/2} i$	km	97 ± 13
Γ		3.4 ± 0.1
f_{scat}		0.43 ± 0.06
χ^2/dof		901/901
Model 3b: CONST×(SIMPL⊗DISKPBB)×SPEXCUT		
Constant		0.72 ± 0.06
kT	keV	1.12 ± 0.03
p		$0.76^{+0.03}_{-0.01}$
N_{diskpbb}		$0.93^{+0.20}_{-0.12}$
$R \cos^{1/2} i$	km	79 ± 10
Γ		1.8 ± 0.1
f_{scat}		0.37 ± 0.03
E_{cut}	keV	$7.5^{+0.8}_{-0.5}$
χ^2/dof		891/900

requires the introduction of an artificially high absorption column density and can result in erroneous determination of the disc properties.

This problem can be solved by using a self-consistent Comptonization model that has a low-energy cutoff in the otherwise power-law-like spectrum, such as the convolution model SIMPL (Steiner et al. 2009), which provides a description of Comptonization based on the non-relativistic theory developed by Sunyaev & Titarchuk (1980). In this model, a fraction of the photons from an input seed spectrum is up-scattered into a power-law component. We therefore modified the single-component Model 3 by including SIMPL, which takes the accretion disc DISKPBB model as an input seed spectrum (SIMPL⊗DISKPBB in XSPEC notation, where ⊗ denotes convolution). This modified model, later referred to as Model 3a, provides an acceptable fit quality ($\chi^2/\text{dof} = 901/901$), as also demonstrated by the residuals (Fig. 5). The best-fitting parameters are listed in Table 4.

As emphasized by Steiner et al. (2009), SIMPL for simplicity does not include any high-energy cutoff. However, any physical thermal Comptonization model should have a cutoff at photon energies higher than kT_e . In order to constrain a possible high-energy attenuation, we added a multiplicative exponential cutoff model SPEXCUT to the convolution model SIMPL⊗DISKPBB (Model 3b in Table 4). The model provides acceptable fit statistics ($\chi^2/\text{dof} = 891/901$), yielding a much harder index $\Gamma = 1.8 \pm 0.1$ and lower scattered photon fraction f_{scat} , and suggests the presence of a high-energy cutoff at $E_{\text{cut}} = 7.5^{+0.8}_{-0.5}$ keV. The improvement in the fit quality is, however, modest, $\Delta\chi^2 \sim 10$ for one fewer degree of freedom, implying that a high-energy cutoff is not strongly demanded by the data (the F-test probability of 2×10^{-3} for null-hypothesis Model 3a). Additionally, we checked that replacing the DISKPBB model by DISKBB gives similar results.

Next, we replaced SIMPL with the more detailed Comptonization model NTHCOMP, where the electron temperature

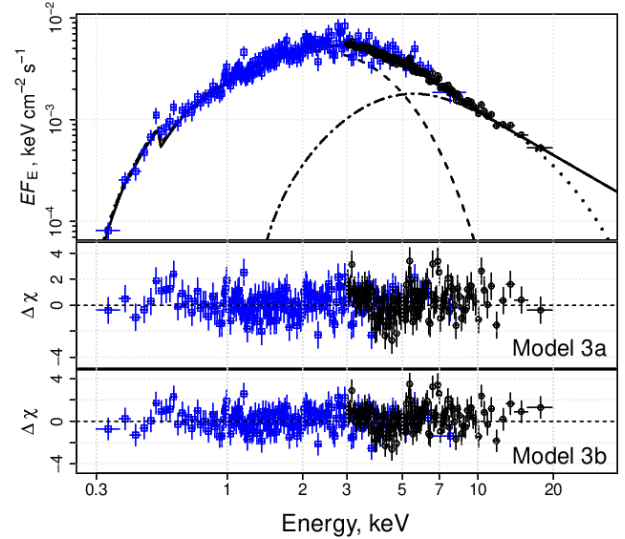


Figure 5. Broad-band *Swift*/XRT and *NuSTAR* spectrum of M33 X-8, shown by blue squares and black circles, respectively. The best-fitting spectral Model 3a (SIMPL⊗DISKPBB, Table 4) is shown by the solid black curve, along with a single accretion disc component DISKPBB ($kT = 0.9 \pm 0.1$ keV, dashed curve) and the difference between the latter and the total model spectrum (i.e. SIMPL⊗DISKPBB–DISKPBB, the dot-dashed curve). The dotted curve represents the best-fitting Model 3b (SIMPL⊗DISKPBB)×SPEXCUT. The two bottom panels show the fit residuals for the respective models.

is a free parameter (Lightman & Zdziarski 1987; Zdziarski et al. 1996; Życki et al. 1999). The NTHCOMP model approximates the Comptonization spectrum with the solution of the Kompaneets equation applying a relativistic correction to the energy transfer between photons and electrons. The input seed photons can be either blackbody or originating from a multi-colour accretion disc. The list of model parameters includes the asymptotic power-law photon index Γ_{nthcomp} , the coronal electron temperature $kT_{e, \text{nthcomp}}$, the seed photon temperature (linked to the inner accretion disc temperature in our case), and the normalization N_{nthcomp} . Fitting by NTHCOMP in combination with a p -free “slim” disc model DISKPBB provides a good fit with $\chi^2/\text{dof} = 886/900$. The model is not sensitive to the high-energy rollover, implying $kT_{e, \text{nthcomp}} > 100$ keV. An alternative combination of the NTHCOMP component with a standard accretion disc DISKBB component constrains the electron temperature to $kT_{e, \text{nthcomp}} = 17.7^{+1.3}_{-2.4}$ keV, at comparable fit statistics ($\chi^2/\text{dof} = 887/901$) for one fewer free parameter. The best-fitting model parameters are listed in Table 5.

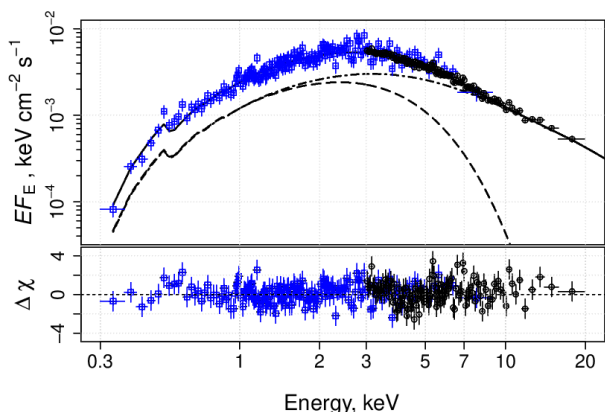
4 DISCUSSION AND CONCLUSIONS

We have analyzed the hard X-ray (3–20 keV) spectrum of M33 X-8 based on the data obtained in 2017 with *NuSTAR* in the framework of the Legacy Program. In order to extend the spectrum into the softer X-ray band, we made use of the high-quality spectrum acquired with *Swift*/XRT during the long observation of M33 X-8 in 2012.

In 2017, the X-ray flux of M33 X-8 in the 0.3–10 keV

Table 5. Same as Table 3, but for Models 6a and 6b.

Parameter	Units	Value
Model 6a: CONST×(DISKBB+NTHCOMP)		
Constant		1.01 ± 0.05
kT	keV	0.93 ^{+0.06} _{-0.03}
p		0.80 ^{+0.03} _{-0.07}
N_{diskbb}		0.44 ^{+0.03} _{-0.06}
$R \cos^{1/2}i$	km	54 ⁺² ₋₄
Γ_{nthcomp}		3.39 ^{+0.07} _{-0.13}
$kT_{\text{e, nthcomp}}$	keV	365 ⁺¹⁰⁰ ₋₂₂₀
N_{nthcomp}	10 ⁻³	1.9 ± 0.3
χ^2/dof		886/900
Model 6b: CONST×(DISKBB+NTHCOMP)		
Constant		1.01 ± 0.05
kT	keV	0.97 ± 0.04
N_{diskbb}		0.40 ± 0.04
$R \cos^{1/2}i$	km	52 ± 3
Γ_{nthcomp}		3.2 ± 0.2
$kT_{\text{e, nthcomp}}$	keV	17.7 ^{+1.3} _{-2.4}
N_{nthcomp}	10 ⁻³	1.5 ± 0.3
χ^2/dof		887/901


Figure 6. Broad-band *Swift*/XRT and *NuSTAR* spectrum of M33 X-8, shown by blue squares and black circles, respectively. The best-fitting spectral Model 6a (DISKBB + NTHCOMP, Table 5) is shown by the solid black curve. The single accretion disc component DISKBB and the Comptonization NTHCOMP component are shown by the dashed and dash-dotted curves, respectively. The bottom panel shows the fit residuals.

energy band (as found by extrapolating the *NuSTAR* spectrum, using Model 3a, to lower energies) was $1.8 \times 10^{-11} \text{ erg s}^{-1} \text{ cm}^{-2}$, which falls into the range of fluxes, $(1.1 - 2.0) \times 10^{-11} \text{ erg s}^{-1} \text{ cm}^{-2}$, observed from this source over a period of 16 years (1998–2014) with *Swift*/XRT and other missions (La Parola et al. 2015). This confirms that M33 X-8 is a relatively stable source compared to some other ULXs. Applying a line-of-sight absorption correction of ~ 15 per cent (inferred from the Galactic value $N_{\text{H}} = 1.1 \times 10^{21} \text{ cm}^{-2}$ Kalberla et al. 2005), to the observed flux, we find that the 0.3–10 keV isotropic luminosity of M33 X-8 is $1.6 \times 10^{39} \text{ erg s}^{-1}$ (for a distance of 817 kpc). The corresponding 3–20 keV luminos-

ity $5.8 \times 10^{38} \text{ erg s}^{-1}$ is almost unaffected by absorption and has been directly measured for M33 X-8 for the first time. The broad-band, 0.3–20 keV, luminosity is $2.2 \times 10^{39} \text{ erg s}^{-1}$ and can be regarded as bolometric in X-rays, because the spectrum falls rapidly above 10 keV. We thus conclude that about 30 per cent of the total luminosity is radiated at energies above 10 keV.

The broad-band (0.3–20 keV) spectrum of M33 X-8 can be well represented by a sum of two distinct components. The first one is a blackbody-like emission with a temperature $\sim 1 \text{ keV}$, which presumably originates in an accretion disc. The second component, detected reliably up to 20 keV, dominates the emission above 10 keV. This hard X-ray tail is well fitted by a power law with a photon index $\Gamma \approx 3$.

In the slim-disc interpretation often used to describe ULX spectra, we find the temperature gradient parameter $p \approx 0.75$ to be perfectly consistent with the value expected for a standard geometrically thin disc (Models 3a/b and 6a, see Tables 4 and 5). Note that a single slim-disc model does not fit the broad-band spectrum, putting the temperature gradient at its hard limit $p = 0.5$ (Model 3, Table 3). This resembles the results obtained by La Parola et al. (2015) using the narrow-band *Swift*/XRT data, who found $p = 0.60 \pm 0.02$. We conclude that the broad-band (0.3–20 keV) spectrum of M33 X-8 does not require a slim-disc interpretation. The normalization of the disc component varies in the wide range 0.4–1.4 between the models, implying the inner disc radius, $R \cos^{1/2}i$, to range between 50 and 100 km, broadly consistent with the compact object being a stellar-mass black hole.

The hard tail can be well approximated by the empirical Comptonization model SIMPL, in which a fraction of seed photons from the accretion disc are scattered into a power-law component. Alternatively, the hard tail can be approximated by more accurate Comptonization models such as NTHCOMP. In both cases, introducing a high-energy cutoff leads to a moderate improvement in the goodness of fit, although the statistical significance of this result is not high.

Overall, in its broad-band spectral properties M33 X-8 resembles black-hole X-ray binaries in their very high (or steep power-law) state. Specifically, the characteristic temperature of the accretion disc is $\sim 1 \text{ keV}$, the hard tail is steep ($\Gamma \sim 3$) and contributes significantly ($\geq 30\%$) to the total luminosity. Furthermore, a number of X-ray binaries have been caught at luminosities $\sim 10^{39} \text{ erg s}^{-1}$ in their very high state (e.g. McClintock & Remillard 2006; Done et al. 2007), similar to the observed luminosity of M33 X-8. All this suggests that M33 X-8 may be a black-hole system accreting at a high but sub-critical rate, in contrast to higher luminosity ULXs, where super-Eddington accretion presumably takes place.

As mentioned in Section 1, the recent discovery of X-ray pulsations from a number of ULXs has demonstrated that in such objects super-Eddington accretion proceeds onto a magnetized neutron star, rather than a black hole. Can M33 X-8 too be an object of this type?

As demonstrated by Walton et al. (2018b), the spectra of ULX-pulsars are similar to those of the majority of well-studied ULXs. Specifically, they peak (when plotted in $E F_E$ units) at 5–10 keV and can be described by a combination of stable thermal emission from an accretion disc and a pulsating non-thermal component that is well fit by

a cutoff power law with $\Gamma \sim 0-1$ and $E_{\text{cut}} \sim 5-20$ keV. The latter presumably originates in accretion columns at the surface of the neutron star. The spectrum of M33 X-8, studied here, can be described by a similar combination of thermal and non-thermal components, with the latter having best-fitting parameters ($\Gamma \sim 1$ and $E_{\text{cut}} \sim 5$ keV) similar to those of ULX-pulsars. However, the contribution of this hard component to the total spectrum is much weaker than in ULX-pulsars. Furthermore, the thermal component, presumably associated with the accretion disc, is softer. As a result, the spectrum of M33 X-8 peaks at a much lower energy, ~ 2.5 keV, and looks quite different from the spectra of ULX-pulsars and from those of the majority of ULXs. This suggests that M33 X-8 is *not* a neutron-star accretor.

Nevertheless, if we interpret the soft component as emission from the accretion disc truncated by a neutron star's magnetic field, the inferred size of the emission region implies that the magnetosphere extends to $\gtrsim 5$ stellar radii. In this case, we would expect an additional harder component coming from the accretion columns at the neutron star surface with luminosity several times higher than the observed soft disc luminosity. Furthermore, the accretion rate will then be a few times higher than that implied by the observed luminosity, i.e. highly supercritical. The actually observed luminosity of the hard component in the spectrum of M33 X-8 is, however, less than half of the total one, which poses a serious problem for the neutron star scenario. It is possible though that the hard X-ray component is weak because the accretion columns are partially obscured by the inner thick disc. In that case, there would be no X-ray pulsations either; and indeed, our and previous (Middleton et al. 2011) searches for pulsations in M33 X-8 have been unsuccessful.

In our view, the interpretation of the data with the model invoking a black hole is preferred. Based on the similarity with the very high state of black-hole X-ray binaries, we may expect the hard spectral tail of M33 X-8 to extend well above 20 keV as, for example, is seen in GRS 1915+105 (Zdziarski et al. 2001). This could be verified with specially dedicated longer *NuSTAR* observations.

ACKNOWLEDGMENTS

This work has made use of data from the *NuSTAR* mission, a project led by the California Institute of Technology, managed by the Jet Propulsion Laboratory and funded by NASA, and observations obtained with *XMM-Newton*, an ESA science mission with instruments and contributions directly funded by ESA Member States and NASA. The research has made use of the *NuSTAR* Data Analysis Software jointly developed by the ASI Science Data Center (ASDC, Italy) and the California Institute of Technology. The data reduction and spectral analysis were performed by RK and SS with the support of grant 14-12-01315 from the Russian Science Foundation. SST and JP took part in the interpretation of the results with the support of grant 14.W03.31.0021 from the Ministry of Education and Science of the Russian Federation.

REFERENCES

- Anders E., Grevesse N., 1989, *Geochim. Cosmochim. Acta*, 53, 197
- Annuar A., et al., 2015, *ApJ*, 815, 36
- Arnaud K. A., 1996, in Jacoby G. H., Barnes J., eds, *ASP Conf. Ser. 101, Astronomical Data Analysis Software and Systems V*. p. 17
- Bachetti M., et al., 2014, *Nature*, 514, 202
- Brightman M., et al., 2016, *ApJ*, 829, 28
- Burrows D. N., et al., 2005, *Space Sci. Rev.*, 120, 165
- Chashkina A., Abolmasov P., Poutanen J., 2017, *MNRAS*, 470, 2799
- Colbert E. J. M., Mushotzky R. F., 1999, *ApJ*, 519, 89
- Done C., Gierliński M., Kubota A., 2007, *A&A Rev.*, 15, 1
- Dubus G., Rutledge R. E., 2002, *MNRAS*, 336, 901
- Dubus G., Charles P. A., Long K. S., Hakala P. J., 1997, *ApJ*, 490, L47
- Dubus G., Charles P. A., Long K. S., 2004, *A&A*, 425, 95
- Evans P. A., et al., 2009, *MNRAS*, 397, 1177
- Fabbiano G., 1989, *ARA&A*, 27, 87
- Fabrika S., 2004, *Astrophysics and Space Physics Reviews*, 12, 1
- Feng H., Soria R., 2011, *New Astron. Rev.*, 55, 166
- Foschini L., Rodriguez J., Fuchs Y., Ho L. C., Dadina M., Di Cocco G., Courvoisier T. J.-L., Malaguti G., 2004, *A&A*, 416, 529
- Fürst F., et al., 2016, *ApJ*, 831, L14
- Gebhardt K., et al., 2001, *AJ*, 122, 2469
- Gehrels N., et al., 2004, *ApJ*, 611, 1005
- Gierliński M., Zdziarski A. A., Poutanen J., Coppi P. S., Ebisawa K., Johnson W. N., 1999, *MNRAS*, 309, 496
- Gottwald M., Pietsch W., Hasinger G., 1987, *A&A*, 175, 45
- Harrison F. A., et al., 2013, *ApJ*, 770, 103
- Isobe N., Kubota A., Sato H., Mizuno T., 2012, *PASJ*, 64, 119
- Israel G. L., et al., 2017a, *Science*, 355, 817
- Israel G. L., et al., 2017b, *MNRAS*, 466, L48
- Kalberla P. M. W., Burton W. B., Hartmann D., Arnal E. M., Bajaja E., Morras R., Pöppel W. G. L., 2005, *A&A*, 440, 775
- Kormendy J., McClure R. D., 1993, *AJ*, 105, 1793
- Krivonos R., Sazonov S., 2016, *MNRAS*, 463, 756
- La Parola V., D'Aí A., Cusumano G., Mineo T., 2015, *A&A*, 580, A71
- Lightman A. P., Zdziarski A. A., 1987, *ApJ*, 319, 643
- Lipunov V. M., 1982, *Soviet Ast.*, 26, 54
- Lipunova G. V., 1999, *Astronomy Letters*, 25, 508
- Long K. S., 1982, *Advances in Space Research*, 2, 177
- Long K. S., Dodorico S., Charles P. A., Dopita M. A., 1981, *ApJ*, 246, L61
- Madsen K. K., et al., 2015, *ApJS*, 220, 8
- Makishima K., et al., 2000, *ApJ*, 535, 632
- Maloney P. R., Begelman M. C., Pringle J. E., 1996, *ApJ*, 472, 582
- Marston A. P., Elmegreen D., Elmegreen B., Forman W., Jones C., Flanagan K., 1995, *ApJ*, 438, 663
- McClintock J. E., Remillard R. A., 2006, in Lewin W. H. G., van der Klis M., eds, *Compact stellar X-ray sources*, Cambridge Astrophysics Series, No. 39. Cambridge University Press, Cambridge, pp 157–213
- Merritt D., Ferrarese L., Joseph C. L., 2001, *Science*, 293, 1116
- Middleton M. J., Sutton A. D., Roberts T. P., 2011, *MNRAS*, 417, 464
- Mineshige S., Hirano A., Kitamoto S., Yamada T. T., Fukue J., 1994, *ApJ*, 426, 308
- Moretti A., et al., 2005, *SPIE*, 5898, 360
- Mukherjee E. S., et al., 2015, *ApJ*, 808, 64
- Mushtukov A. A., Suleimanov V. F., Tsygankov S. S., Poutanen J., 2015, *MNRAS*, 454, 2539
- Mushtukov A. A., Suleimanov V. F., Tsygankov S. S., Ingram A.,

- 2017, MNRAS, 467, 1202
- Mushtukov A. A., Tsygankov S. S., Suleimanov V. F., Poutanen J., 2018, MNRAS, 476, 2867
- Poutanen J., Lipunova G., Fabrika S., Butkevich A. G., Abolmasov P., 2007, MNRAS, 377, 1187
- Rana V., et al., 2015, ApJ, 799, 121
- Roberts T. P., Middleton M. J., Sutton A. D., Mezcua M., Walton D. J., Heil L. M., 2016, Astronomische Nachrichten, 337, 534
- Sazonov S. Y., Lutovinov A. A., Krivonos R. A., 2014, Astronomy Letters, 40, 65
- Schulman E., Bregman J. N., 1995, ApJ, 441, 568
- Shakura N. I., Sunyaev R. A., 1973, A&A, 24, 337
- Shidatsu M., Ueda Y., Fabrika S., 2017, ApJ, 839, 46
- Steiner J. F., Narayan R., McClintock J. E., Ebisawa K., 2009, PASP, 121, 1279
- Sunyaev R. A., Titarchuk L. G., 1980, A&A, 86, 121
- Sutton A. D., Swartz D. A., Roberts T. P., Middleton M. J., Soria R., Done C., 2017, ApJ, 836, 48
- Takano M., Mitsuda K., Fukazawa Y., Nagase F., 1994, ApJ, 436, L47
- Trinchieri G., Fabbiano G., Peres G., 1988, ApJ, 325, 531
- Tüllmann R., et al., 2011, ApJS, 193, 31
- Walton D. J., et al., 2013, ApJ, 779, 148
- Walton D. J., et al., 2014, ApJ, 793, 21
- Walton D. J., et al., 2015a, ApJ, 799, 122
- Walton D. J., et al., 2015b, ApJ, 806, 65
- Walton D. J., et al., 2016, ApJ, 827, L13
- Walton D. J., et al., 2017, ApJ, 839, 105
- Walton D. J., et al., 2018a, MNRAS, 473, 4360
- Walton D. J., et al., 2018b, ApJ, 856, 128
- Weng S.-S., Wang J.-X., Gu W.-M., Lu J.-F., 2009, PASJ, 61, 1287
- Winkler C., et al., 2003, A&A, 411, L1
- Zdziarski A. A., Gierliński M., 2004, Prog. Theor. Phys. Suppl., 155, 99
- Zdziarski A. A., Johnson W. N., Magdziarz P., 1996, MNRAS, 283, 193
- Zdziarski A. A., Grove J. E., Poutanen J., Rao A. R., Vadawale S. V., 2001, ApJ, 554, L45
- Zycki P. T., Done C., Smith D. A., 1999, MNRAS, 309, 561

This paper has been typeset from a $\text{\TeX}/\text{\LaTeX}$ file prepared by the author.